High-Resolution Spatio-Temporal Model for County-Level COVID-19 Activity in the U.S.

SHIXIANG ZHU, ALEXANDER BUKHARIN, LIYAN XIE, MAURICIO SANTILLANA, SHIHAO YANG, and YAO XIE

We present an interpretable high-resolution spatio-temporal model to estimate COVID-19 deaths together with confirmed cases 1 week ahead of the current time, at the county level and weekly aggregated, in the United States. A notable feature of our spatio-temporal model is that it considers the (1) temporal auto- and pairwise correlation of the two local time series (confirmed cases and deaths from the COVID-19), (2) correlation between locations (propagation between counties), and (3) covariates such as local within-community mobility and social demographic factors. The within-community mobility and demographic factors, such as total population and the proportion of the elderly, are included as important predictors since they are hypothesized to be important in determining the dynamics of COVID-19. To reduce the model's high dimensionality, we impose sparsity structures as constraints and emphasize the impact of the top 10 metropolitan areas in the nation, which we refer to (and treat within our models) as *hubs* in spreading the disease. Our retrospective out-of-sample county-level predictions were able to forecast the subsequently observed COVID-19 activity accurately. The proposed multivariate predictive models were designed to be highly interpretable, with clear identification and quantification of the most important factors that determine the dynamics of COVID-19. Ongoing work involves incorporating more covariates, such as education and income, to improve prediction accuracy and model interpretability.

CCS Concepts: • Applied computing \rightarrow Health care information systems; Health informatics; Forecasting;

Additional Key Words and Phrases: COVID-19, spatio-temporal model, vector autoregressive process

ACM Reference format:

Shixiang Zhu, Alexander Bukharin, Liyan Xie, Mauricio Santillana, Shihao Yang, and Yao Xie. 2021. High-Resolution Spatio-Temporal Model for County-Level COVID-19 Activity in the U.S.. *ACM Trans. Manag. Inform. Syst.* 12, 4, Article 33 (September 2021), 20 pages.

https://doi.org/10.1145/3468876

1 INTRODUCTION

The global spread of COVID-19, the disease caused by the novel coronavirus SARS-CoV-2, has affected nearly everyone's lives on the planet. Even the largest economies' resources have been

The paper is partially supported by NSF CAREER CCF-1650913, NSF DMS-1938106 and DMS-1830210 $\,$

Authors' addresses: S. Zhu, A. Bukharin, L. Xie, S. Yang, and Y. Xie, 755 Ferst Dr NW, Atlanta, GA 30332; emails: shixiang. zhu@gatech.edu, abukharin3@gatech.edu, lxie49@gatech.edu, shihao.yang@isye.gatech.edu, yao.xie@isye.gatech.edu; M. Santillan, Computational Health Informatics Program, Boston Children's Hospital 1 Autumn Street, Office 451Boston, MA 02115; email: msantill@g.harvard.edu.

Permission to make digital or hard copies of all or part of this work for personal or classroom use is granted without fee provided that copies are not made or distributed for profit or commercial advantage and that copies bear this notice and the full citation on the first page. Copyrights for components of this work owned by others than ACM must be honored. Abstracting with credit is permitted. To copy otherwise, or republish, to post on servers or to redistribute to lists, requires prior specific permission and/or a fee. Request permissions from permissions@acm.org.

© 2021 Association for Computing Machinery.

2158-656X/2021/09-ART33 \$15.00

https://doi.org/10.1145/3468876

33:2 S. Zhu et al.

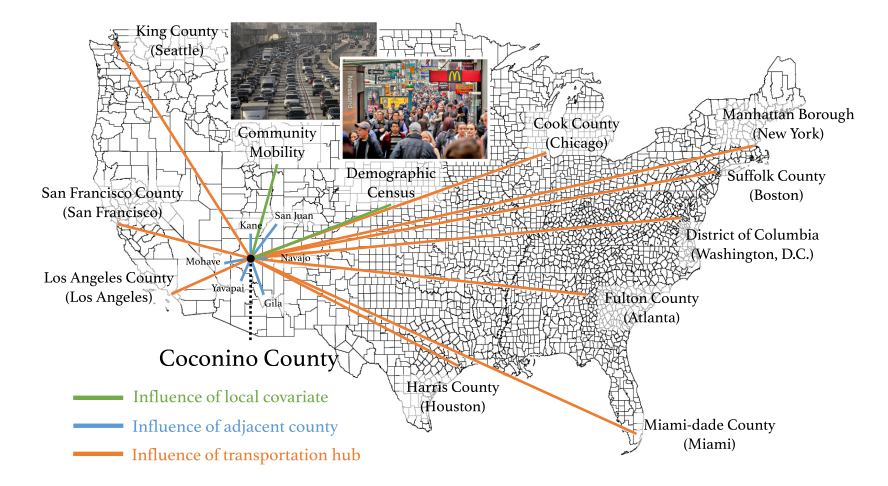


Fig. 1. An example of spatio-temporal covariates in our model for Coconino County, Arizona. Based on the counties in the United States as fundamental units, we assume the number of confirmed cases and deaths of COVID-19 reported in a given county are jointly related to the numbers reported in its adjacent counties (they are Kane, San Juan, Navajo, Gila, Yavapai, and Mohave for Coconino in this example) and 10 selected nationwide hubs (including San Francisco, Los Angeles, Seattle, Chicago, Atlanta, Miami, Washington, D.C., Boston, and New York). The numbers of cases and deaths also depend on some local covariates, such as community mobility level and some counties' demographic factors.

strained due to the large infectivity and transmissibility of COVID-19. As the number of cases of COVID-19 continues increasing, understanding the finer-grained spatio-temporal dynamics of this disease and some of the leading factors affecting disease transmissions is critical to helping officials make policy decisions and curb further spread of the disease.

Most of the previous research aimed at studying the spread of COVID-19 has focused on two key measurements: the number of confirmed cases and the number of deaths. Cases going up or down over time shed light on the rate of spread of COVID-19 at a given point in time—but it is only valid if enough people get tested. The limited testing ability resulted in a severe underestimation of COVID-19 cases in the pandemic's early stages [35]. For example, when there was not enough testing capacity, as was the case in New York City in March 2020, the number of cases reported was an undercount of actual cases, estimated to be much larger (up by a factor of 10) [23, 40]. Some studies have circumvented underestimation by considering the case positivity rate, which measures the percentage of total COVID-19 tests conducted that are positive. However, most of the widely used COVID-19 datasets, such as the COVID Tracking Project [48], only collect the total number of people with a completed polymerase chain reaction (PCR) test that returns positive as reported by the state or territory, which has a much lower spatial resolution (state level) in comparison with the case and death data (county level). Such coarse-grained testing numbers would introduce extra noise to our model and would most likely be incapable of improving the confirmed case prediction accuracy at the county level. Deaths are also an important metric that most people care about regarding the virus's ultimate epidemiological impact. In contrast to the number of confirmed cases, the number of deaths is a good and accurate indicator for evaluating how serious a burden this pandemic is causing, not only on health care systems but also on the general public's mental health and well-being. Some epidemiological studies, such as [33], also recommend tracking deaths, even though deaths lag behind new cases, typically by 2 weeks to a month.

A large amount of fine-grained data offers a unique opportunity to study the disease's spread dynamics from a micro-level view. For the United States, several teams have been working on collecting comprehensive COVID-19 tracking data, including daily counts of cases and deaths at the county level. Such data gives us a general picture of how the virus is spreading across metropolitan and micropolitan counties and how such dynamics are evolving. Besides considering the cases and the deaths, we also aim to study other critical local factors in transmitting COVID-19. Recent studies [38] on the spread of COVID-19 show that besides the distance to the epicenter, other factors, such as subway and airport, are positively connected with the virus transmission. Moreover, both urban areas and population density are positively associated with the spread of COVID-19 after the outbreak. The proportion of the elderly population has also been identified as a key factor in the death rate. Therefore, we consider the within-community mobility and two critical demographic factors by taking advantage of the COVID-19 Community Mobility Reports [21] and the American Community Survey (ACS) [8]. These two datasets are publicly available and include detailed county-level statistics that provide insights into what has changed in response to policies aimed at combating COVID-19 and what factors may affect the disease's transmission. As illustrated in Figure 1, in our model, we assume the numbers of cases and deaths in each county depend on the neighboring counties and major metropolitan areas in the United States, which we refer to as hubs in spreading the disease. Local community mobility and demographic factors, including population and elderly population, are considered local covariates in the model, which also play a crucial role in the final number of deaths.

In this article, we use a data-driven method incorporating a large-scale dataset from multiple sources to predict the deaths and the confirmed cases of COVID-19 at the county level in the United States. Since death is a more accurate indicator for assessing the spread of the virus, we emphasize predicting county-level deaths' trajectories instead of the confirmed cases. Our method's most notable contribution is considering the spatial structure among hubs and neighboring counties in modeling the cross-correlation between cases and deaths. We also present the effect of a wide variety of geographic community mobility and social demographic factors on the spread of COVID-19. Our approach drastically differs from previous studies [1, 6, 14], in which the number of cases and deaths, and other covariates, including the community mobility and social demographic factors, are interlinked through a vector autoregressive process. Our model shows that these hubs play a pivotal role in spreading the disease. We also find that both cases and deaths are significantly related to the local level's total population and that deaths are also positively associated with the proportion of the elderly population. Additionally, we found that confirmed cases are not significantly related to the proportion of the elderly population, which may prove that the disease was mostly circulating among young people in its later stage. In particular, while we identify a spike in cases since the beginning of the summer, we do not observe a clear spike in deaths. This may be explained by the fact that a more significant proportion of young people, who are generally at lower risk of death, were infected in the more recent pandemic stages.

The remainder of the article is organized as follows. We first review related works in the rest of this section, followed by describing the datasets we have used in Section 2. Section 3 presents our proposed vector autoregressive model with spatial structure incorporated. We demonstrate the effectiveness of our model and discuss its interpretation in Section 4. Lastly, the article concludes with discussions and future research directions in Section 5.

Related Work. Compartmental models have been widely used in infectious disease epidemiological studies. In the SIR model [22], one of the simplest compartmental models, the population is assigned to three components: S (susceptible), I (infectious), and R (recovered). These variables (S, I, and R) represent the number of people in each compartment. The transition between different compartments is modeled using a set of coupled differential equations. Based on the SIR

33:4 S. Zhu et al.

model, many variants have been proposed in the last decades, including the **SIRD** (**Susceptible-Infectious-Recovered-Deceased**) model [9, 18] that considers deceased individuals, and the **SEIR** (**Susceptible-Exposed-Infectious-Recovered**) model [25–27, 44, 59] that considers the exposed period during which individuals have been infected but are not yet infectious themselves, to name a few. The total population is usually assumed to be fixed in the compartmental models; therefore, it works well when modeling nationwide data. However, in our high-resolution modeling, each county's population is of high variability due to dynamics across the county. Therefore, we use a spatio-temporal model instead to capture the influence of major big cities and neighboring counties without fixing each county's population.

Besides compartmental models, much work has been done on predicting the total number of COVID-19 cases and deaths without considering the spatial correlation across regions [39, 56, 58]. For example, recent work [7] introduces a regional model based on a self-exciting point process to forecast the total number of infections for multiple countries. Another work [20] provides a state-wise analysis and infections prediction for India's states by considering three growth models, namely, the logistic, the exponential, and the susceptible-infectious-susceptible models. Machine-learning-based approaches have also been considered in modeling COVID-19 outbreak [3]. Some work [55] attempts to use a neural network to model accumulative case counts for multiple countries. Recurrent-neural-network-based methods [24, 60] have been applied to model the temporal dynamics of the COVID-19 outbreak. Our approach differs from these studies in two ways: (1) our model provides finer-grained predictions for the cases and deaths; (2) we model the multivariate time series by considering the spatial correlation across regions as well as the correlation with the demographic factors, which is more interpretable than the machine-learning-based methods.

Understanding the COVID-19 outbreak's spatial spread is critical to predicting local outbreaks and developing public health policies during the early stages of COVID-19. However, studies evaluating the spatial spread of the COVID-19 pandemic are scarce or limited [46]. Previous studies have described the spatial spread of **severe acute respiratory syndrome (SARS)** in Beijing and mainland China [15, 17, 29, 30, 42] using limited or localized data. One study also considered the various connections between a few cities to calculate the spatial association [42]. There is also prior work using the multivariate Hawkes process to model the conditional intensity of new COVID-19 cases and deaths in the United States at the county level [12], without considering the influence of the big cities and other important demographic factors. The work of [4] develops two types of county-level predictive models based on the exponential and the linear model, respectively. It focuses on modeling the dynamics of cumulative death counts. In [31], the graph neural networks are adopted to capture the spatio-temporal dynamics between various features; however, the lack of interpretability hinders further understanding of the mechanism of the COVID-19 outbreak.

There is also a wide array of previous research based on autoregressive models that relate to our work. In [2, 5, 16, 34, 50, 53], the **autoregressive integrated moving average (ARIMA)** is used to predict future data for different countries. [41] uses an autoregressive-based time series model to predict the total number of the world's confirmed cases. [11, 51] adopt the autoregressive artificial neural networks to predict the number of accumulative cases in Egypt. A more recent similar article [32] studies the state-wise cases in Pakistan using the vector autoregressive model. However, two significant differences are (1) the spatial resolution of their predictions is much lower than our results, and (2) these models do not consider the spatial correlation between places in the vicinity and cities served as major transportation hubs.

There are also various efforts studying impacts from other aspects, such as temperature, humidity [47, 52], age, gender [15], and travel restrictions [13, 36]. Here, in our case, $N = I \times T = 157, 200$. Most of these studies are constrained on a relatively small scale because of limited data at the pandemic's early stage.

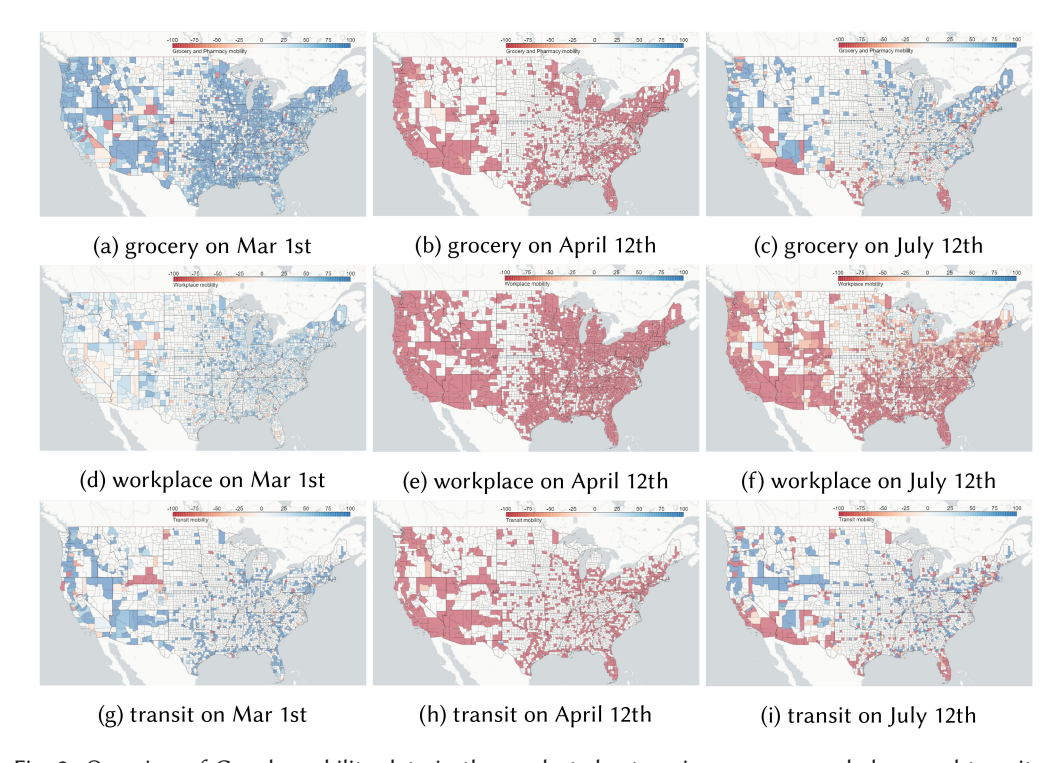


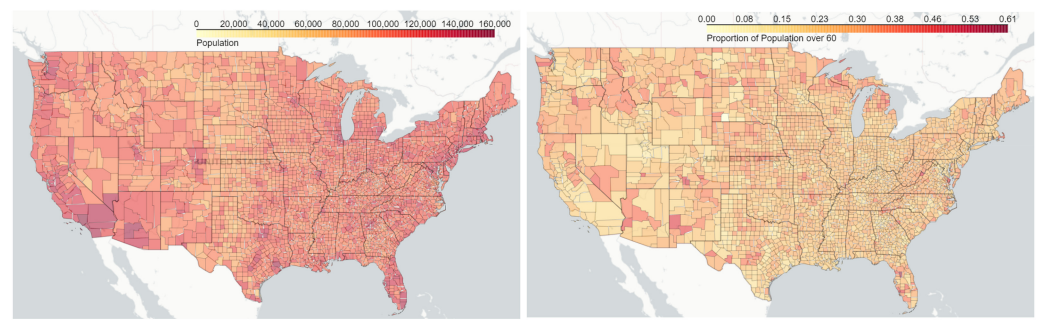
Fig. 2. Overview of Google mobility data in three selected categories: grocery, workplace, and transit on three different days. Counties in red and blue indicate their mobility is lower and higher than the normal level, respectively. The mobility level varies over time and space due to local government policy change in response to COVID-19.

2 DATA

We have used three comprehensive datasets in this study, including confirmed cases and deaths of COVID-19, community mobility data, and demographic census data. These datasets play an important role in understanding the spatio-temporal correlation of COVID-19 transmission.

Confirmed Cases and Deaths of COVID-19. We used the dataset from The New York Times [57], based on state and local health agencies' reports. The data is the product of dozens of journalists working across several time zones to monitor news conferences, analyze data releases, and seek public officials' clarification on how they categorize cases. The data includes two parts: (1) Confirmed cases are counts of individuals whose coronavirus infections were confirmed by a laboratory test and reported by a federal, state, territorial, or local government agency. Only tests that detect viral RNA in a sample are considered confirmatory. These are often called molecular or reverse transcription-polymerase chain reaction (RT-PCR) tests. (2) Confirmed deaths are individuals who have died and meet the definition for a confirmed COVID-19 case. Some states reconcile these records with death certificates to remove deaths from their count, where COVID-19 is not listed as the cause of death. These data have removed non-COVID-19 deaths among confirmed cases according to the information released by health departments, i.e., in homicides, suicides, car crashes, or drug overdoses. All cases and deaths are counted on the date they are first announced. In practice, we have observed periodic weekly oscillations in daily reported cases and deaths, which could have been caused by testing bias (higher testing rates on certain days of the week). To reduce such bias, we aggregate the number of cases and deaths of each county by week.

33:6 S. Zhu et al.



- (a) county-level total population
- (b) county-level proportion of elderly population

Fig. 3. Overview of the social demographic factors. The color depth represents the value of the demographic variables of interest in certain counties.

Community Mobility. As global communities respond to COVID-19, we have heard from public health officials that the same type of aggregated, anonymized insights we use in products such as Google Maps could be helpful as they make critical decisions to combat COVID-19. The COVID-19 Community Mobility Reports [21] aim to provide insights into what has changed in response to policies aimed at combating COVID-19. The reports record people's movement by county daily, across various categories such as retail and recreation, groceries and pharmacies, parks, transit stations, workplaces, and residential. The data shows how visitors to (or time spent in) categorized places change compared to the baseline days (in percentage). The negative percentage represents that the level of mobility is lower than the baseline, and the positive percentage represents the opposite. A baseline day represents a normal value for that day of the week. The baseline day is the median value from the 5 weeks from January 3 to February 6, 2020. To match the temporal resolution with the COVID-19 data and detrend the weekly pattern, we aggregate each county's mobility data by week. Examples of three categories have been shown in Figure 2. Figure 3 shows two leading factors that affect the spread and infection of the disease, i.e., total population and the proportion of the elderly aged 65 or older [45].

Demographic Census. Data from the ACS [8], provided by the U.S. Census Bureau, is a comprehensive source for demographic information about the population, age, and economic status in each zip code region in the United States. Unlike the census data, which takes place every 10 years, the ACS is conducted every year. The latest ACS data are available in the year 2018. Some demographic factors help us understand how population distribution affects the spread of disease (by correlating the local socio-economic profile with its confirmed cases and deaths). These factors contain essential information about the development and economic growth of different areas. To match the spatial resolution with the COVID-19 data, we aggregate the zip code regions' demographic data in the same county. We selected two leading factors that affect the spread and the infection of the disease, i.e., total population and the proportion of the elderly aged 65 or older [45].

3 METHODOLOGY

This section presents our statistical model that captures the spatio-temporal correlation of the spread of COVID-19. We begin with a brief description of the problem setup and notations, then jointly model confirmed cases and deaths as a vector autoregressive process in Section 3.2. The essential notations defined in this section are also summarized in Table 1.

Section	Notation	Description						
3.1	$\mathcal{T} = \{t = 1, \dots, T\}$	Set of all weeks.						
	$\mathcal{I} = \{i = 1, \ldots, N\}$	Set of all counties.						
	$\mathcal{K} = \{k = 1, \dots, K\}$	Set of mobility categories.						
	$\mathcal{L} = \{k = 1, \dots, L\}$	Set of demographic factors.						
	$c_{i,t} \in \mathbb{Z}_+$	Number of confirmed cases for county $i \in I$ in week $t \in \mathcal{T}$.						
	$d_{i,t} \in \mathbb{Z}_+$	Number of deaths for county $i \in I$ in week $t \in \mathcal{T}$.						
	$z_{i,l} \in \mathbb{R}_+$	Data of demographic factor $l \in \mathcal{L}$ for county $i \in \mathcal{I}$.						
	$m_{i,k,t}\in\mathbb{R}$	Data of mobility category $k \in \mathcal{K}$ for county $i \in I$ in week $t \in \mathcal{T}$.						
3.2	$\mathcal{A} = \{(i,j): i,j \in I\}$	Set of all county pairs in the U.S. that i , j are adjacent to each other or one of i , j is a hub .						
	$\boldsymbol{B}_{\tau} = (\beta_{i,j}) \in \mathbb{R}^{N \times N}$	Case's coefficients depended on past confirmed cases between county $i, j \in \mathcal{I}$ for τ weeks ago.						
	$A_{\tau} = (\alpha_{i,i}) \in \mathbb{R}^{N \times N}$	Death's coefficients depended on past deaths between county $i, j \in I$ for τ weeks ago.						
	$H_{\tau} = (h_{i,j}) \in \mathbb{R}^{N \times N}$	Death's coefficients depended on past confirmed cases between county $i, j \in I$ for τ weeks ago.						
	$\mu_{k, au}\in\mathbb{R}$	Coefficient for mobility category $k \in \mathcal{K}$ in the past τ -th week w.r.t. the number of cases.						
	$v_{k,\tau} \in \mathbb{R}$	Coefficient for mobility category $k \in \mathcal{K}$ in the past τ -th week w.r.t. the number of deaths.						
	$v_I \in \mathbb{R}$	Coefficient for demographic factor $l \in \mathcal{L}$ w.r.t. the number of cases.						
	$\zeta_l \in \mathbb{R}$	Coefficient for demographic factor $l \in \mathcal{L}$ w.r.t. the number of deaths.						

Table 1. Summary of Essential Notations

3.1 Problem Setup and Notations

Consider confirmed cases and deaths of COVID-19 in N counties and T weeks (recall that we aggregated these numbers by week to reduce bias). Let $I = \{i = 1, \ldots, N\}$ be the set of counties and $\mathcal{T} = \{t = 1, \ldots, T\}$ be the set of weeks starting from March 15, 2020 until January 17, 2021. We assume there is a set of counties $I' = \{i = 1, \ldots, N'\} \subset I$ playing a significant role in spreading the disease due to their high population density and well-developed transportation network connecting to other major cities in the United States. We refer to these counties as hubs, and the selected hubs are marked in Figure 1. Denote the number of confirmed cases and deaths in county $i \in I$ and week $t \in \mathcal{T}$ as $c_{i,t} \in \mathbb{Z}_+$ and $d_{i,t} \in \mathbb{Z}_+$, respectively. In our setting, T = 49, N = 3,144, and N' = 10.

We also consider K mobility categories and L demographic factors as covariates of the model, where K=6 and L=2. Let $\mathcal{K}=\{k=1,\ldots,K\}$ be the set of community mobility categories and $\mathcal{L}=\{l=1,\ldots,L\}$ be the set of demographic factors. Denote the mobility score in category $k\in\mathcal{K}$ for county $i\in I$ in week $t\in\mathcal{T}$ as $m_{i,k,t}\in\mathbb{R}$, and denote the data of demographic factor $l\in\mathcal{L}$ for county $i\in I$ as $z_{i,l}\in\mathbb{R}_+$. Let $c_t:=[c_{1,t},\ldots,c_{N,t}]^\intercal$ and $d_t:=[d_{1,t},\ldots,d_{N,t}]^\intercal$ denote the confirmed cases and deaths in week $t\in\mathcal{T}$, respectively. Let $m_{k,t}:=[m_{1,k,t},\ldots,m_{N,k,t}]^\intercal$ denote the score of community mobility category $k\in\mathcal{K}$ for all counties $i\in I$ in week $t\in\mathcal{T}$. Let $z_l:=[z_{1,l},\ldots,z_{N,l}]^\intercal$ denote the data of demographic factor $l\in\mathcal{L}$ for all counties $i\in I$.

3.2 Spatio-Temporal Vector Autoregressive Model

We consider a linear spatio-temporal autoregressive model where the number of confirmed cases (c_t) and deaths (d_t) is a time series regressed on their previous values and the mobility covariate $m_{k,t}$ and demographic covariate z_l . Denote the time window's length that we consider in the past (the memory depth) as p. Based on previous studies [54], it is known that the COVID-19 virus has an incubation period of around 2 weeks. Therefore, we choose p = 2 throughout this article.

Define the augmented observation vector as (which contains both confirmed case and death counts):

$$\mathbf{x}_t \coloneqq \begin{bmatrix} \mathbf{c}_t \\ \mathbf{d}_t \end{bmatrix} \in \mathbb{R}^{2N}.$$

Then our spatio-temporal model can be written as a vector autoregressive (VAR) process:

$$\boldsymbol{x}_{t} = \sum_{\tau=1}^{p} \Lambda_{\tau} \boldsymbol{x}_{t-\tau} + \sum_{k=1}^{K} \sum_{\tau=1}^{p} \boldsymbol{\gamma}_{k,\tau} \otimes \boldsymbol{m}_{k,t-\tau} + \sum_{l=1}^{L} \omega_{l} \otimes \boldsymbol{z}_{l} + \boldsymbol{\epsilon}_{t}, \quad \boldsymbol{\epsilon}_{t} \sim \mathcal{N} \left(\boldsymbol{0}, \begin{bmatrix} \Sigma_{\eta} & \boldsymbol{0} \\ \boldsymbol{0} & \Sigma_{\eta} \end{bmatrix} \right), \quad (1)$$

ACM Transactions on Management Information Systems, Vol. 12, No. 4, Article 33. Publication date: September 2021.

33:8 S. Zhu et al.

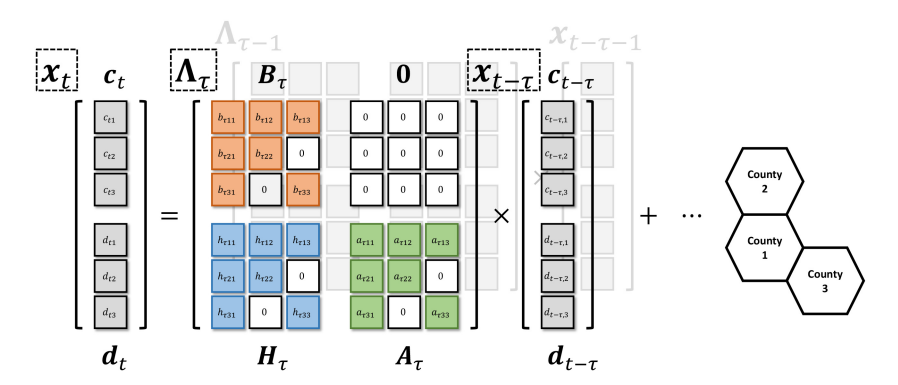


Fig. 4. A small illustrative example of spatial factor matrices with three counties. The adjacency of these counties is shown on the right. In this example, the observation x_t is six-dimensional and the matrices A_{τ} , H_{τ} , and B_{τ} are all three-by-three matrices. The white boxes represent zero entries; the gray boxes represent data entries (cases and deaths); the red, the blue, and the green boxes represent the learnable (non-zero) entries in matrix B_{τ} , H_{τ} , A_{τ} , respectively.

where \otimes is the Kronecker product and

$$\boldsymbol{\Lambda}_{\tau} = \begin{bmatrix} \boldsymbol{B}_{\tau} & \boldsymbol{0} \\ \boldsymbol{H}_{\tau} & \boldsymbol{A}_{\tau} \end{bmatrix} \in \mathbb{R}^{2N \times 2N}, \; \boldsymbol{\gamma}_{k,\tau} = \begin{bmatrix} \mu_{k,\tau} \\ v_{k,\tau} \end{bmatrix} \in \mathbb{R}^2, \; \boldsymbol{\omega}_{l} = \begin{bmatrix} v_{l} \\ \zeta_{l} \end{bmatrix} \in \mathbb{R}^2, \; \boldsymbol{\epsilon}_{t} = \begin{bmatrix} \boldsymbol{\epsilon}_{t,c} \\ \boldsymbol{\epsilon}_{t,d} \end{bmatrix} \in \mathbb{R}^{2N}, \; 1 \leq \tau \leq p.$$

In our model in Equation (1), the first term captures the dependence on past confirmed cases and deaths; the second term captures the influence of past local community mobility; the third term captures the influence of local demography, which is held constant over time. Specifically, B_{τ} and A_{τ} contain the autoregressive coefficients for the number of confirmed cases and deaths, respectively; H_{τ} describes the dependence of the current number of deaths on the number of confirmed cases τ weeks ago. As an illustrative example shown in Figure 4, these three matrices share the same sparse structure, where the entry at (i, j) is zero if county i and county j are not adjacent and none of them is the hub. Formally, the set of adjacency pairs is defined by \mathcal{A} $\{(i,j)\in I: (i,j) \text{ is an edge of the graph } \mathcal{G}\}$; each node of \mathcal{G} denotes a county, and there is an edge between two nodes whenever the corresponding counties are geographically adjacent or one of them is a hub. The $\mu_{k,\tau}$, $\nu_{k,\tau}$, ν_l , and ζ_l are four scalar coefficients. To be specific, $\mu_{k,\tau}$, $\nu_{k,\tau}$ represent the coefficients for the local community mobility score in category $k \tau$ weeks ago with respect to the corresponding number of confirmed cases and deaths, respectively. Similarly, v_l , ζ_l represent the coefficients for local demographic factor l with respect to the corresponding number of confirmed cases and deaths, respectively. The spatial covariance matrix between the noise at counties i and j is denoted as the (i, j)-th entry of Σ_n ; it is a function of their Euclidean distance s_{ij} and is parameterized by η . Some commonly used spatial models include the Gaussian model [37], Exponential model [19], and Matérn model [19]. Here we adopt the exponential spatial covariance model $\Sigma_{\eta}(i,j) = \eta \exp\{-\eta s_{ij}\}\$, where η is a pre-specified parameter, which controls the rate of spatial decay. In this article, we specify a reasonable value of the parameter $\eta = 10^3$.

We aim to fit the model in Equation (1) for confirmed cases and deaths jointly by minimizing the *prediction error*. Define the set of parameters $\theta = \{\Lambda, \omega, \gamma\} \in \Theta$, where Θ is the set containing all feasible values. For a pre-specified hyper-parameter $\delta \in [0, 1]$, the loss function is defined as a weighted combination of quadratic loss functions for death and confirmed case residuals:

$$\ell(\boldsymbol{\theta}) := \delta \sum_{t=1}^{T} \boldsymbol{\varepsilon}_{t,d}^{\mathsf{T}} \boldsymbol{\Sigma}_{\eta}^{-1} \boldsymbol{\varepsilon}_{t,d} + (1 - \delta) \sum_{t=1}^{T} \boldsymbol{\varepsilon}_{t,c}^{\mathsf{T}} \boldsymbol{\Sigma}_{\eta}^{-1} \boldsymbol{\varepsilon}_{t,c}, \tag{2}$$

where $\varepsilon_{t,c}$ denotes the confirmed case prediction residual

$$\boldsymbol{\varepsilon}_{t,c} = \begin{bmatrix} I & \mathbf{0} \end{bmatrix} \left(\boldsymbol{x}_t - \sum_{\tau=1}^p \boldsymbol{\Lambda}_{\tau} \boldsymbol{x}_{t-\tau} - \sum_{k=1}^K \sum_{\tau=1}^p \boldsymbol{\gamma}_{k,\tau} \otimes \boldsymbol{m}_{k,t-\tau} - \sum_{l=1}^L \boldsymbol{\omega}_l \otimes \boldsymbol{z}_l \right),$$

and $\varepsilon_{t,\mathrm{d}}$ denotes the death prediction residual

$$\boldsymbol{\varepsilon}_{t,\mathrm{d}} = \begin{bmatrix} \mathbf{0} & I \end{bmatrix} \left(\boldsymbol{x}_t - \sum_{\tau=1}^p \boldsymbol{\Lambda}_{\tau} \boldsymbol{x}_{t-\tau} - \sum_{k=1}^K \sum_{\tau=1}^p \boldsymbol{\gamma}_{k,\tau} \otimes \boldsymbol{m}_{k,t-\tau} - \sum_{l=1}^L \boldsymbol{\omega}_l \otimes \boldsymbol{z}_l \right).$$

The hyper-parameter δ controls the proportion of death prediction loss. In practical terms, we emphasize the importance of death, and hence we choose $\delta = 0.9$ empirically. The reason is that it is known that the confirmed cases are quite noisy and can depend on the capacity of testings.

The parameters θ can be estimated by solving the following optimization with a regularization function:

$$\min_{\theta \in \Theta} \ell(\theta) + \lambda_1 R(\theta),\tag{3}$$

where $\lambda_1 \ge 0$ is a parameter that controls the importance of the regularization term, and $R(\theta)$ is the elastic net type regularization function (with hyper-parameter $\lambda_2 \in [0, 1]$) given by

$$R(\boldsymbol{\theta}) := \sum_{\tau=1}^{p} \sum_{i=1}^{N} \sum_{j=1}^{N} \mathbb{1}_{\mathcal{A}} \left\{ (i,j) \right\} \left[\lambda_{2} \left(|\alpha_{i,j,\tau}| + |\beta_{i,j,\tau}| + |h_{i,j,\tau}| \right) + (1 - \lambda_{2}) \left(|\alpha_{i,j,\tau}|^{2} + |\beta_{i,j,\tau}|^{2} + |h_{i,j,\tau}|^{2} \right) \right],$$

where $\mathbb{1}_A\{x\}$ is the indicator function, i.e., taking the value 1 if $x \in A$, otherwise 0; λ_2 is the ℓ_1 penalty ratio in the regularization function; $\alpha_{i,j,\tau}, \beta_{i,j,\tau}, h_{i,j,\tau}$ are the entries of matrices $A_{\tau}, B_{\tau}, H_{\tau}$, respectively.

3.3 Exploit Sparsity and Structure to Solve Large-Scale Optimization Problems

Our model's most salient feature is that we consider the underlying spatio-temporal structure between the number of confirmed cases and deaths. If there is no specific structure in coefficient matrices, our methods look on the surface to be a naive linear model but require to solve a large-scale high-dimensional optimization problem, which contains 79,077,916 parameters (variables in the optimization problem) with only 84,888 data points. Instead of solving such complex problems directly, we tackle this challenge by exploiting the sparse spatial structure and only consider the correlation between adjacent counties and hubs, which leads to a significant reduction in the number of parameters (less than 80,000). Besides, the lower triangular structure of the Λ_{τ} matrix (including B_{τ} , H_{τ} , and A_{τ}) captures the causal relationship we believe exists in the confirmed case to the death count, but not the other way around. To be exact, we assume the number of confirmed cases in the past will result in the change of both the confirmed cases and deaths in the future, while the number of deaths only relates to the future's deaths.

The regularization term we devised in Section 3.2 also plays a big part in achieving the ideal results. This elastic net-based method linearly combines the lasso and ridge regression penalties on B_{τ} , H_{τ} , and A_{τ} to encourage sparse spatial correlation and stabilize the solution at the same time. The hyper-parameters λ_1 and λ_2 in the regularization term are chosen by fivefold cross-validation, where the optimal choices are $\lambda_1 \approx 10^2$ and $\lambda_2 \approx 10^{-1}$ for the fitted model.

Here we solve the optimization problem by gradient descent. To fit the model, we first standardize the data of covariates and feed all the data as a single batch in one iteration, then descend the gradients of the parameters with respect to the loss defined in Equation (2) until the model converges. To perform a 1-week-ahead prediction, we feed all the data before that week as a single

33:10 S. Zhu et al.

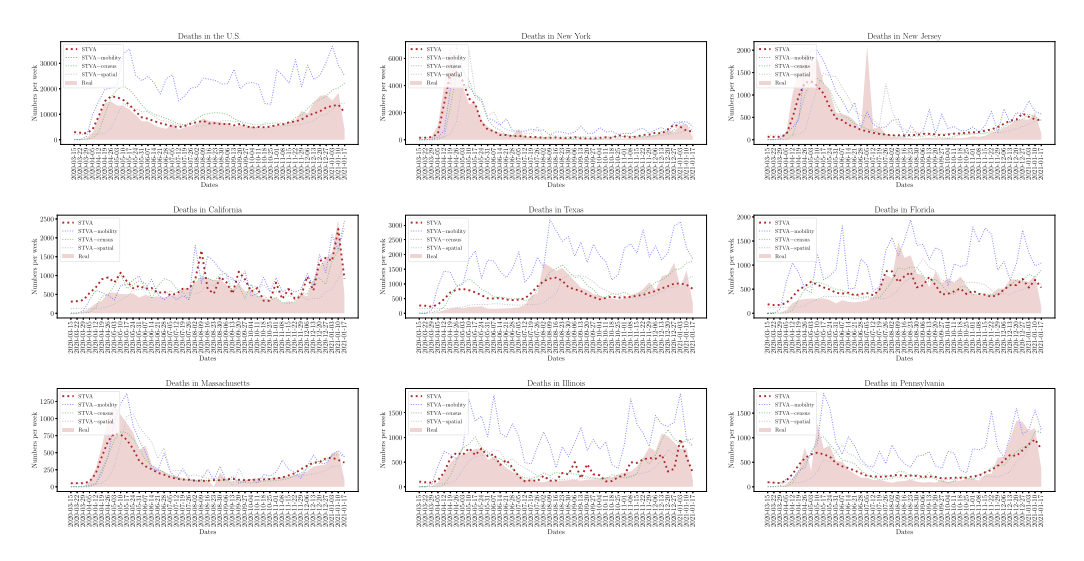


Fig. 5. In-sample estimated deaths (red dotted lines) for the United States and other eight major states with the highest number of COVID-19 deaths in the United States. Figures are sorted in descending order of the total number of deaths since March 15, 2020. The results show that our model can capture the general dynamics of the death numbers.

batch in one iteration and follow the same gradient descent procedure described above. The model normally takes about 500 iterations to reach the convergence with $\ell(\theta) \approx 1.41 \times 10^3$.

4 RESULTS

Now we report the results of our study. We evaluate the explanatory power of the proposed modeling method by performing the in-sample estimation. We also compare our approach regarding the 1-week-ahead predictive performance against four other external benchmark methods, which are the current state-of-the-art methods adopted by the **Centers for Disease Control and Prevention (CDC)** in its national ensemble forecast [10, 49]. We generate the death (and case) prediction for each county in a week by taking the past county-level case and death records, community mobility, and demographic census information as input. The format of the input data is described in Section 2. In addition, we demonstrate the interpretable components of our model by showing the spatio-temporal correlation between the number of COVID-19 cases and other covariates discovered from our fitted model. For the ease of presentation, we only focus on the mainland and do not consider Hawaii, Alaska, and other unincorporated territories of the United States in this article. Hereinafter, we refer to the proposed spatio-temporal vector autoregressive model as STVA.

4.1 Model Evaluation

4.1.1 In-Sample Estimation. To evaluate the effectiveness of our method, we compare the county-level in-sample estimation on the number of deaths. The in-sample estimation is a process of evaluating the model's explanatory capabilities using observed data to see how effective the model is in reproducing the data. The process can be carried out as follows: We first fit the model using the entire dataset from March 15, 2020, to January 17, 2021, which contains 3,144 counties and 49 weeks in total. The in-sample estimation can then be obtained by feeding the same data into the fitted model and recovering the estimation for deaths according to Equation (1). We also carry out three ablation studies to further investigate the effectiveness of each model component. To be specific, we consider three variant models: (1) STVA—mobility removes the component of

	13445	Pct. MAE	MAE for	Pct. MAE	MAE for	Pct. MAE	MAE for	Pct. MAE
	I MAE	Increase ¹	COVID-19 1st Peaks ²	Increase	COVID-19 2nd Peaks ³	Increase	Most Affected Region ⁴	Increase
STVA	1.63	N/A	0.31	N/A	2.96	N/A	10.35	N/A
STVA-spatial	1.99	18.09%	0.94	67.02%	3.24	8.64%	14.19	27.06%
STVA-census	2.45	33.47%	0.66	53.03%	4.43	33.18%	15.65	33.87%
STVA-mobility	5.73	71.55%	2.10	85.23%	7.97	62.86%	12.91	19.83%

Table 2. Quantitative Comparison of MAE between our STVA and Other Ablation Models

mobility (the second term in Equation (1)); (2) STVA-census removes the component of demographic census (the third term in Equation (1)); and (iii) STVA-spatial simply removes the spatial correlation (the first term in Equation (1)) by a diagonal matrix. We note that each county can also be regarded as an independent auto-regressive (AR) model without spatial correlation. We report the in-sample estimation of the proposed approach and the ablation models by aggregating the county-level estimated numbers in the same state. As shown in Figure 5, we select eight major states with the highest total number of deaths in the United States. The shaded area indicates the actual number of deaths reported in the COVID-19 dataset, and the solid red line indicates the in-sample estimated deaths by our model. We observe that the STVA (solid red lines) can capture the dynamics of true death trajectories better than the other three ablation models (dashed lines). We also provide quantitative results for county-level **mean absolute error (MAE)** in Table 2. As we can see, the result indicates that our model STVA generally attains the lowest MAE for all scenarios. There are also significant performance gains if we only focus on predicting the peak week and the most affected region in the United States. The result suggests that these components are conducive to improving the model's performance. In Appendix A, we also present the in-sample estimation of the confirmed cases for the same eight states.

4.1.2 Out-of-Sample Prediction. In addition to the in-sample estimation, we assess the model's predictive power by performing the 1-week-ahead (out-of-sample) prediction. The prediction procedure withholds the future data from the model estimation, then uses the fitted model to make predictions for the (hold-out) data in the next week.

Here, we compare our model against four benchmark methods adopted by the CDC, which represent the current state-of-the-art for COVID-19 prediction: (1) COVID-19 Mortality Projections for the U.S. States by the University of Texas, Austin (UT) [56, 58]: they introduce a negative-binomial mixed-effects **generalized linear model (GLM)**—i.e., the predictor is a GLM with a logarithm link function; (2) COVID-19 Cases and Deaths Forecasts by the Los Alamos National Laboratory (LANL) [39]: the model assumes that a fraction of the newly generated cases will die and proposes a statistical model to capture this effect; (3) COVID-19 Modeling by the Northeastern University, Laboratory for the Modeling of Biological and Socio-technical Systems (MOBS) [44]: their team adopts a classic SLIR-like compartmentalization scheme for disease progression; (4) COVID-19 Projections for the United States by the Institute for Health Metrics and Evaluation (IHME) [27, 28]: this project considers a deterministic SEIR compartmental framework. In particular, all four approaches mainly use the state-level records of the number of cases and deaths as the input of their models. At the same time, IHME also takes advantage of several critical driving covariates (pneumonia seasonality, mobility, testing rates, and mask use per capita). The prediction results of these benchmark methods are directly quoted from the CDC's official reports [10].

¹Pct. MAE Increase is the percentage of increased MAE that results by removing one of the components in STVA.

 $^{^{2}}$ COVID-19 1st Peaks refers to a certain time period (4 weeks from April 5, 2020, to May 3, 2020) in which the number of deaths in the United States reaches its first peak.

³ COVID-19 2nd Peaks refers to a certain time period (4 weeks from December 13, 2020, to January 3, 2021) in which the number of deaths in the United States reaches its second peak.

⁴Most Affected Region refers to the region of eight states with the highest number of deaths due to COVID-19, including New York, New Jersey, California, Texas, Florida, Massachusetts, Illinois, and Pennsylvania.

33:12 S. Zhu et al.



Fig. 6. One-week-ahead death prediction for the United States and other eight major states with the highest number of COVID-19 deaths in the United States. The STVA's statewise predictions are obtained by aggregating the county-level predictions in the same states. Figures are sorted in descending order of the total number of confirmed cases since October 11, 2020. The results show that our model can achieve promising predictive performance with the other four benchmarks. Note that these four benchmarks only provide state-level predictions.

We only present the results from October 11, 2020, for 1-week-ahead death prediction. The statistics before October are inaccurate due to the low testing rate, and the data are insufficient to fit the model. Similar to the in-sample estimation, we report the prediction results for the entire United States and eight top states with the highest number of deaths in Figure 6. It shows that the aggregated county-level predictions suggested by the STVA (solid green lines) achieve competitive performance against other mainstream approaches (dash lines). It is worth noting that these four methods only provide state-level forecasting for the number of deaths, which is less challenging than the county-level prediction.

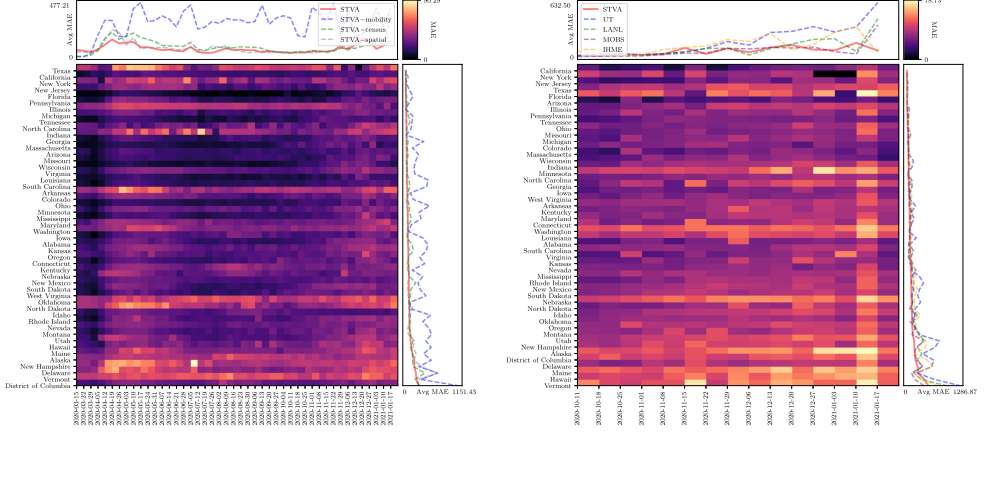
More quantitative results are summarized in Figure 7. The heatmaps show the MAE of the county-level estimation/prediction within a particular state and at certain weeks. The average MAEs over states and weeks are presented in the vertical line chart on the right and the horizontal line chart on the top. The states are sorted in ascending order of their MAE from top to bottom. As shown in Figure 7, our model significantly outperforms the other ablation models while achieving competitive predictive performances compared to the other widely adopted state-level approaches. We can also observe that our model tends to achieve better performance for the states with larger populations, such as Florida, New York, Texas, and so forth; for the deaths, our model has a balanced performance in each state, and the MAE is getting better (smaller) and becoming more stable after the summer surge of COVID-19 (from June to July).

4.2 Model Interpretation

Our study focuses on exploring the in-sample explanatory content of predetermined factors in our model. We fit the model using the entire dataset collected from three data sources mentioned in Section 2 and interpret the model by examining its fitted coefficients.

Spatio-Temporal Dependencies between Cases and Deaths. The experimental results demonstrate a distinctive underlying spatio-temporal pattern between confirmed cases and deaths of COVID-19.

ACM Transactions on Management Information Systems, Vol. 12, No. 4, Article 33. Publication date: September 2021.



(a) in-sample estimation

(b) one-week ahead (out-of-sample) prediction

Fig. 7. Mean absolute error (MAE) of (a) the in-sample death estimation and (b) the 1-week-ahead out-of-sample death prediction by our model. The color depth of the heatmaps indicates the MAE of county-level prediction for certain states and weeks. The horizontal and vertical line charts show the average MAE over weeks and states comparing to other benchmark methods. The states have been sorted in ascending order of their MAE from top to bottom. Note that four benchmarks in (b) only provide state-level predictions; we compare our method against these benchmarks by summing up the death numbers in the same state.

We first report the coefficients of five representative hubs in Λ_1 in Figure 8. The hubs' coefficients in B_1 , H_1 , A_1 reveal their spatial dependencies between each pair of past cases and current cases, past cases and current deaths, and past deaths and current deaths, respectively. As we can see, hubs have a strong "radiating" power on most of the U.S. regions and contribute a great deal to promote or curb the spread of COVID-19. However, the rural area with lower population density in the central United States is not significantly influenced by the hubs. The hubs situated in the northern United States (e.g., Chicago, New York) are negatively related to spreading diseases to the other regions (in blue), which appear to have better controls on the expansion of the virus. In contrast, the hubs in the southern United States (e.g., Dallas, Houston, Miami) usually are positively related to the increases of both cases and deaths in other regions (in red). The result also presents some other interesting findings: some hubs show two opposite influences on the cases and deaths in the same region. For example, we see that on the one hand, Figure 8(m) shows that the number of deaths in Miami is negatively related to the deaths in the New England area of the United States. On the other hand, Figure 8(n) shows that the number of cases in Miami is positively related to the cases in the same area. Some hubs contribute to the increase of cases or deaths in one region, reducing the cases or deaths in other regions. For example, Figures 8(g) and (j) show that Dallas and Houston have a positive impact on the New England area in the United States and have a negative impact on Florida and California. Apart from analyzing the spatial structure across regions learned by the model, we also study the temporal dependencies in the past 2 weeks for the same hub. In Figure 9, we present three typical pairs of comparisons for coefficients between 1-week lag and 2-week lag: coefficients of Atlanta in A_1 and A_2 , coefficients of Seattle in B_1 and B_2 , and coefficients of Los Angeles in H_1 and H_2 . All three comparisons share one thing in common: coefficients of different time lags have a similar spatial pattern, but the overall coefficients of 2-week lag are relatively smaller than corresponding ones of 1-week lag. This indicates that the last week has a stronger influence. We also observe that the spatial patterns in A, B, and H are significantly

33:14 S. Zhu et al.

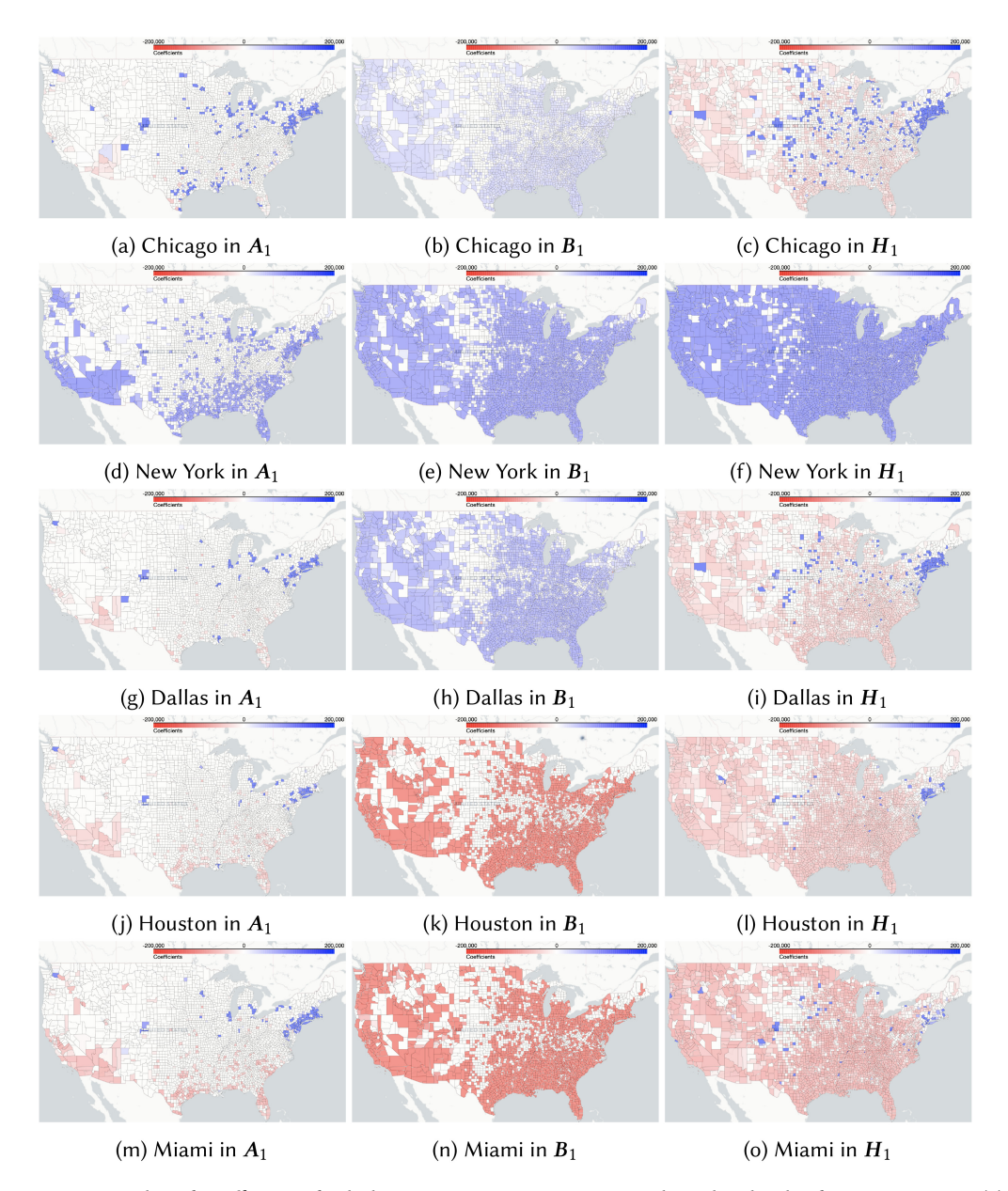


Fig. 8. Examples of coefficients for hubs in matrix Λ_1 . For instance, the color depth of any county i in (a) represents the value of coefficient $\alpha_{i,j,1}$ in A_1 , where county j is Chicago. Counties in blue indicate their current number of deaths is positively related to its number of deaths in the last week; counties in red are the opposite; counties in white represent no discernable correlation between the two numbers. Coefficients of different hubs show the various spatial pattern in "spreading" or "controlling" the disease.

different from each other according to Figure 8 and Figure 9. This observation confirms that each spatial component described by matrices *A*, *B*, and *H* plays a different role in capturing the spatial correlation. For example, we can observe that the visualization of the matrix *H* always shows large positive coefficients in the New England area, while the coefficients in matrix *B* in the same area

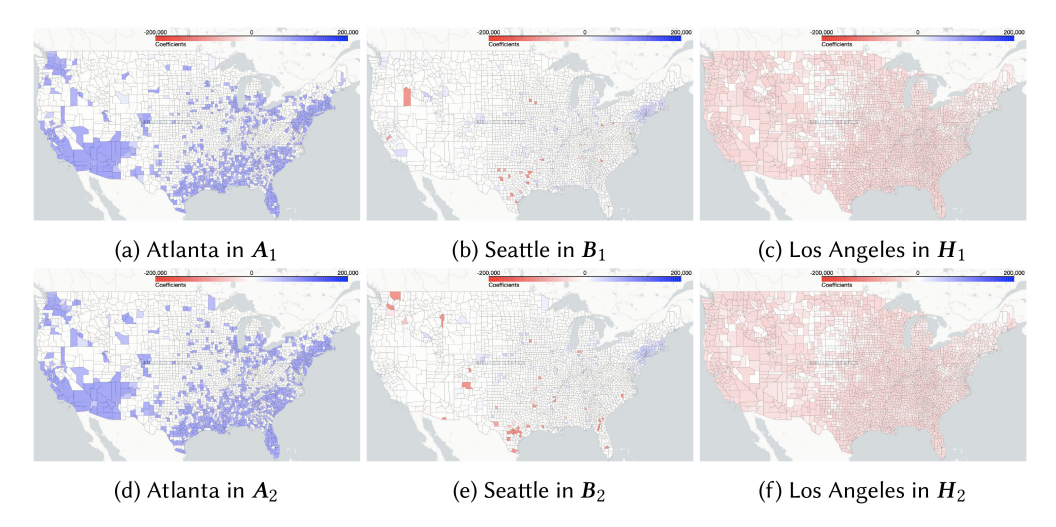


Fig. 9. Examples of coefficients with different time lags.

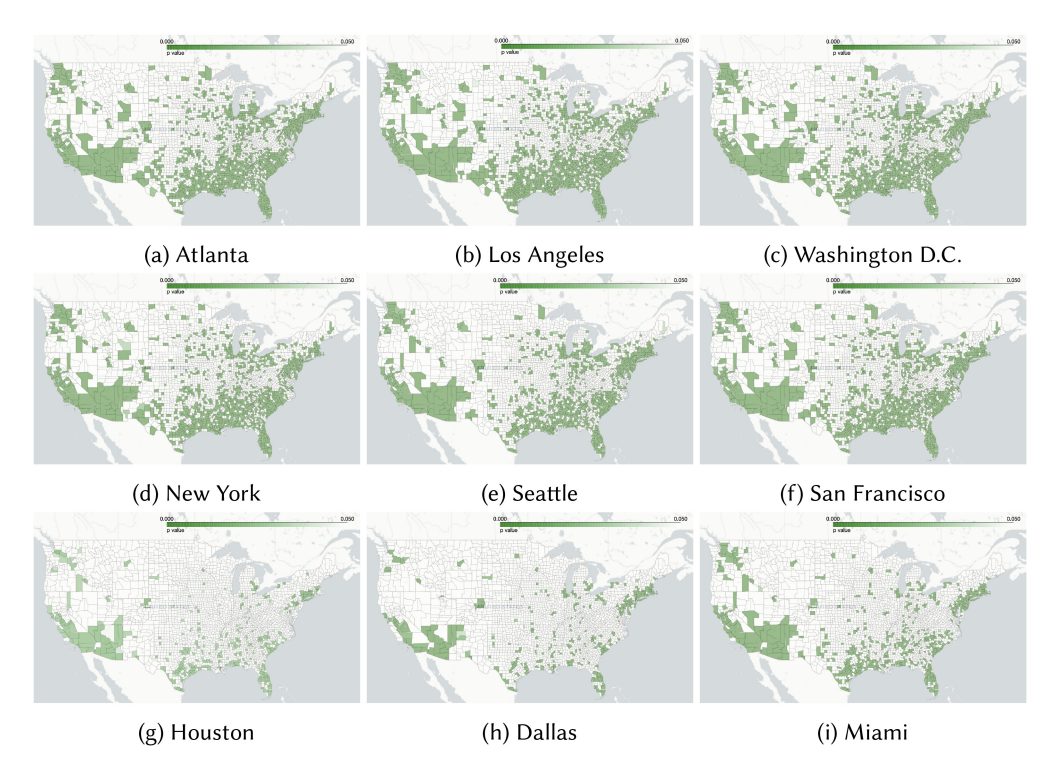


Fig. 10. Examples of p-values for hubs' coefficients in A_1 .

are typically more negligible or even negative. This may be related to the high death rate in the New England area [43] since \boldsymbol{H} captures the spatial correlation between previous cases and future deaths, and \boldsymbol{B} only concerns the similar correlation between cases. Last but not least, we further investigate the p-values of these spatial coefficients, as finding statistically significant relationships between the prediction and the observation is of great importance to the model evaluation. Since

33:16 S. Zhu et al.

Lag	One-Week							Two-Week						N/A
Category	Workplaces	Recreation	Grocery	Park	Transit	Residential	Workplaces	Recreation	Grocery	Park	Transit	Residential	Population	Over 65
Term w.r.t. case	$\mu_{1,1}$	$\mu_{2,1}$	$\mu_{3,1}$	$\mu_{4,1}$	$\mu_{5,1}$	$\mu_{6,1}$	$\mu_{1,2}$	$\mu_{2,2}$	$\mu_{3,2}$	$\mu_{4,2}$	$\mu_{5,2}$	$\mu_{6,2}$	v_1	v_2
Coefficient	+9.67e+2	+1.67e+3	-1.21e+3	-7.83e+2	+3.54e+2	-5.08e+3	+1.28+e3	+2.16e+3	-8.52e+2	-7.25e+2	+3.12e+3	-5.05e+3	+2.91e+4	-1.58e+01
p-value	+5.01e-5	+3.21e-5	+1.03e-7	+7.46e-5	+2.01e-5	+2.56e-5	+2.19e-5	+2.30e-5	+3.77e-7	+3.91e-7	+1.42e-7	+6.64e-7	+9.10e-9	+1.81e-1
t-value	+5.78e+1	+7.63e+1	+1.00e+2	+1.29e+1	-7.26e+1	-5.09e+1	-4.68e+1	-4.33e+1	+2.11e+2	+1.86e+2	-3.03e+2	-3.02e+2	+1.73e+3	-9.42e-1
Term w.r.t. death	$\nu_{1, 1}$	$\nu_{2,1}$	$\nu_{3,1}$	$\nu_{4,1}$	$\nu_{5,1}$	$\nu_{6,1}$	$\nu_{1,2}$	$\nu_{2,2}$	$\nu_{3,2}$	$\nu_{4,2}$	$\nu_{5,2}$	$\nu_{6,2}$	ζ1	ζ_2
Coefficient	-1.92e+3	-1.09e+3	+3.61e+2	+1.17e+3	-3.12e+3	+4.77e+3	-1.55e+3	-9.95e+2	+2.54e+2	+1.15e+3	-3.19e+3	+4.64e+3	-1.68e+4	-1.17e+3
p-value	+2.81e-6	+4.01e-6	+1.97e-5	+7.78e-5	+4.50e-5	+9.21e-5	+1.03e-5	+3.21e-5	+8.09e-7	+3.14e-6	+9.03e-7	+9.67e-7	+1.56e-7	+6.85e-5
t-value	-1.11e+2	-9.00e+1	-6.31e+1	-5.76e+1	+2.09e+1	+1.47e+1	+6.80e+1	+6.66e+1	-1.80e+2	-1.84e+2	+2.76e+2	+2.68e+2	-9.71e+2	-6.70e+1

Table 3. Summary of Fitted Coefficients for Mobility and Demographic Factors

 A_1 plays a key role in predicting future deaths by being connected to the death observations in the past, we take the hubs' coefficients in A_1 as an example. As shown in Figure 10, the number of deaths in these hubs is statistically significant to the death counts in other populated regions in the United States (New England, the southeastern United States, and the western United States). In particular, we find the hubs in the West and the North (Los Angeles, Washington, D.C., New York, Seattle, and San Francisco) are statistically significant to a broader area than the hubs in the South (Houston, Dallas, and Miami).

Dependence on Local Covariates. Table 3 summarizes the fitted coefficients of local covariates in the model. The first and second rows indicate the corresponding time lag and the category of coefficients, respectively. The first 12 columns correspond to the community mobility, and the last two columns correspond to the demographic factors. Positive coefficients have been put in bold to highlight the positive correlation with cases or deaths. The coefficients can be compared across factors as the covariates are standardized first. As we can see, most of the covariates are statistically significant, with small p-values (<.05), except for the proportion of the elderly population aged 65 and older. The positive coefficients are in bold, which indicates a positive correlation between the covariates and the cases or deaths. In particular, we observe that, for the cases, the coefficients of mobility in workplaces, retail, recreation, and transit stations have large positive values $(>9 \times 10^2)$, which indicates that the increase of mobility in these areas led to the rapid spread of COVID-19. However, things are the opposite for the deaths, where the coefficients of mobility in grocery and pharmacies, parks, and residential have large positive values ($>2 \times 10^2$). Moreover, the population's coefficient for the cases is significantly larger than the other covariates, and it confirms that population density is the dominant factor in spreading the disease. Last, we have found that the proportion of the elderly population is significantly related to the deaths and has no clear connection to the cases.

5 DISCUSSION

While still in the development stages, the proposed spatio-temporal model has shown immense promise in modeling and predicting the deaths and confirmed cases of COVID-19 in the United States. Nevertheless, there remain numerous open questions and room for improvements. For example, the uncertainty in the count data commonly exists and can affect accuracy. It would be interesting to incorporate the serology data as an additional data source to calibrate our model. To avoid negative output, we may adapt the current problem into a Poisson regression with the log-linear model or apply a **Rectified Linear Unit (ReLU)** to the output to disallow the negative values. It assumes the response variable x_t has a Poisson distribution and assumes the logarithm of its expected value can be modeled by the linear model defined in Equation (1). In particular, this adaption plays a vital role in predicting states with fewer confirmed cases and deaths, such as Hawaii and Delaware.

APPENDIX

A OTHER NUMERICAL RESULTS

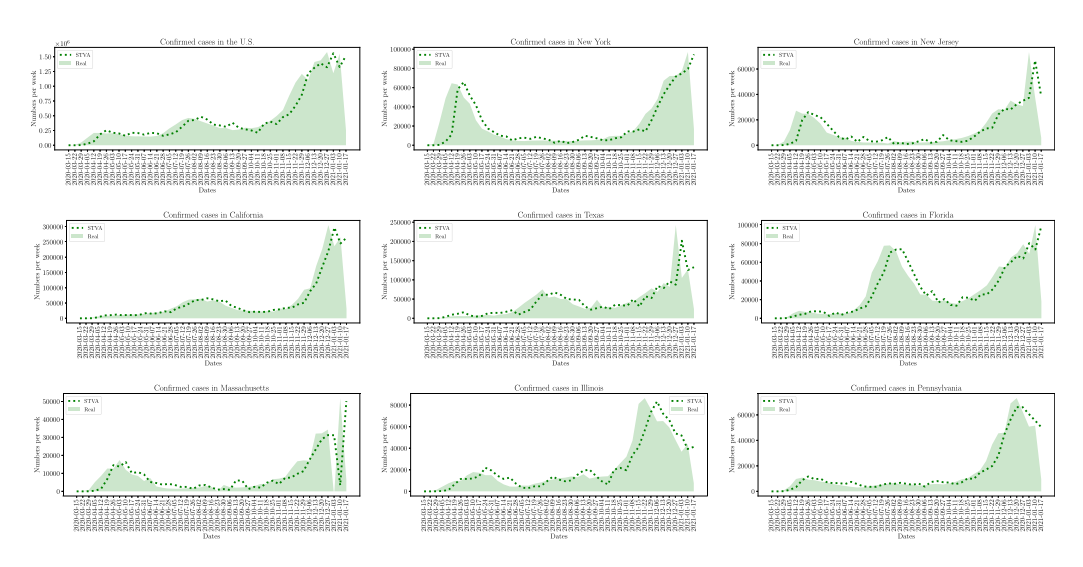


Fig. 11. In-sample estimated cases (green dotted lines) for the United States and other eight major states with the highest number of COVID-19 deaths in the United States. Figures are sorted in descending order of the total number of deaths since March 15, 2020.

ACKNOWLEDGMENTS

The authors would like to thank helpful suggestions from Dr. Brian M. Gurbaxani at CDC.

REFERENCES

- [1] Jérôme Adda. 2016. Economic activity and the spread of viral diseases: Evidence from high frequency data. *Quarterly Journal of Economics* 131, 2 (Feb. 2016), 891–941. https://doi.org/10.1093/qje/qjw005
- [2] Arianna Agosto and Paolo Giudici. 2020. A Poisson autoregressive model to understand COVID-19 contagion dynamics. *Risks* 8, 3 (2020), 77.
- [3] Moutaz Alazab, Albara Awajan, Abdelwadood Mesleh, Ajith Abraham, Vansh Jatana, and Salah Alhyari. 2020. COVID-19 prediction and detection using deep learning. *International Journal of Computer Information Systems and Industrial Management Applications* 12 (2020), 168–181.
- [4] Nick Altieri, Rebecca L. Barter, James Duncan, Raaz Dwivedi, Karl Kumbier, Xiao Li, Robert Netzorg, Briton Park, Chandan Singh, Yan Shuo Tan, Tiffany Tang, Yu Wang, Chao Zhang, and Bin Yu. 2020. Curating a COVID-19 data repository and forecasting county-level death counts in the united states. arXiv preprint arXiv:2005.07882 (2020).
- [5] Saleh I. Alzahrani, Ibrahim A. Aljamaan, and Ebrahim A. Al-Fakih. 2020. Forecasting the spread of the COVID-19 pandemic in saudi arabia using ARIMA prediction model under current public health interventions. *Journal of Infection and Public Health* 13, 7 (2020), 914–919.
- [6] Duygu Balcan, Vittoria Colizza, Bruno Gonçalves, Hao Hu, José J. Ramasco, and Alessandro Vespignani. 2009. Multiscale mobility networks and the spatial spreading of infectious diseases. Proceedings of the National Academy of Sciences 106, 51 (Dec. 2009), 21484–21489. https://doi.org/10.1073/pnas.0906910106
- [7] Andrea L. Bertozzi, Elisa Franco, George Mohler, Martin B. Short, and Daniel Sledge. 2020. The challenges of modeling and forecasting the spread of COVID-19. Proceedings of the National Academy of Sciences 117, 29 (2020), 16732–16738.
- [8] The U.S. Census Bureau. 2019. American Community Survey. https://www.census.gov/programs-surveys/acs.
- [9] Diego Caccavo. 2020. Chinese and Italian COVID-19 outbreaks can be correctly described by a modified SIRD model. medRxiv (April 2020). https://doi.org/10.1101/2020.03.19.20039388
- [10] Centers for Disease Control and Prevention. 2021. COVID-19 Forecasts: Deaths. https://www.cdc.gov/coronavirus/2019-ncov/covid-data/forecasting-us.html#state-forecasts.
- [11] Tanujit Chakraborty, Arinjita Bhattacharyya, and Monalisha Pattnaik. 2020. Theta autoregressive neural network model for COVID-19 outbreak predictions. *medRxiv* (2020).

33:18 S. Zhu et al.

[12] Wen-Hao Chiang, Xueying Liu, and George Mohler. 2020. Hawkes process modeling of COVID-19 with mobility leading indicators and spatial covariates. *medRxiv* (2020).

- [13] Matteo Chinazzi, Jessica T. Davis, Marco Ajelli, Corrado Gioannini, Maria Litvinova, Stefano Merler, Ana Pastore y Piontti, Kunpeng Mu, Luca Rossi, Kaiyuan Sun, et al. 2020. The effect of travel restrictions on the spread of the 2019 novel coronavirus (COVID-19) outbreak. Science 368, 6489 (April 2020), 395–400. https://doi.org/10.1126/science.aba9757
- [14] Vittoria Colizza, Alain Barrat, Marc Barthélemy, and Alessandro Vespignani. 2006. The role of the airline transportation network in the prediction and predictability of global epidemics. *Proceedings of the National Academy of Sciences* 103, 7 (Feb. 2006), 2015–2020. https://doi.org/10.1073/pnas.0510525103
- [15] Chinese Center for Disease Control Epidemiology Working Group for NCIP Epidemic Response and Prevention. 2020. The epidemiological characteristics of an outbreak of 2019 novel coronavirus diseases (COVID-19) in China. Zhonghua liu Xing Bing Xue za zhi = Zhonghua Liuxingbingxue Zazhi 41, 2 (Feb. 2020), 145–151. https://doi.org/10.3760/cma.j.issn.0254-6450.2020.02.003
- [16] Ferdian Fadly and Erika Sari. 2020. An approach to measure the death impact of Covid-19 in Jakarta using autoregressive integrated moving average (ARIMA). *Unnes Journal of Public Health* 9, 2 (2020), 108–116.
- [17] Li-Qun Fang, Sake J. De Vlas, Dan Feng, Song Liang, You-Fu Xu, Jie-Ping Zhou, Jan Hendrik Richardus, and Wu-Chun Cao. 2009. Geographical spread of SARS in mainland China. *Tropical Medicine & International Health* 14, s1 (Oct. 2009), 14–20. https://doi.org/10.1111/j.1365-3156.2008.02189.x
- [18] Jesús Fernández-Villaverde and Charles I. Jones. 2020. Estimating and Simulating a SIRD Model of COVID-19 for Many Countries, States, and Cities. Working Paper 27128. National Bureau of Economic Research. https://doi.org/10.3386/ w27128
- [19] Carlo Gaetan and Xavier Guyon. 2010. Spatial Statistics and Modeling. Vol. 90. Springer, New York, NY. https://doi.org/ 10.1007/978-0-387-92257-7
- [20] Palash Ghosh, Rik Ghosh, and Bibhas Chakraborty. 2020. COVID-19 in India: Statewise analysis and prediction. JMIR Public Health and Surveillance 6, 3 (2020), e20341.
- [21] Google. 2020. COVID-19 Community Mobility Reports. https://www.google.com/covid19/mobility/.
- [22] Tiberiu Harko, Francisco S.N. Lobo, and M.K. Mak. 2014. Exact analytical solutions of the susceptible-infected-recovered (SIR) epidemic model and of the SIR model with equal death and birth rates. Appled Mathematics and Computation 236 (June 2014), 184–194. https://doi.org/10.1016/j.amc.2014.03.030
- [23] Fiona P. Havers, Carrie Reed, Travis Lim, Joel M. Montgomery, John D. Klena, Aron J. Hall, Alicia M. Fry, Deborah L. Cannon, Cheng-Feng Chiang, Aridth Gibbons, et al. 2020. Seroprevalence of antibodies to SARS-CoV-2 in 10 sites in the United States, March 23-May 12, 2020. JAMA Internal Medicine 180, 12 (Jul. 2020), 1576–1586. https://doi.org/10.1001/jamainternmed
- [24] Mohamed Hawas. 2020. Generated time-series prediction data of COVID-19's daily infections in brazil by using recurrent neural networks. *Data in Brief* 32 (2020), 106175.
- [25] Herbert W. Hethcote. 2000. The mathematics of infectious diseases. SIAM Review 42, 4 (Oct. 2000), 599–653. https://doi.org/10.1137/S0036144500371907
- [26] Can Hou, Jiaxin Chen, Yaqing Zhou, Lei Hua, Jinxia Yuan, Shu He, Yi Guo, Sheng Zhang, Qiaowei Jia, Chenhui Zhao, Jing Zhang, Guangxu Xu, and Enzhi Jia. 2020. The effectiveness of quarantine of Wuhan city against the Corona Virus Disease 2019 (COVID-19): A well-mixed SEIR model analysis. Journal of Medical Virology 92, 7 (April 2020), 841–848. https://doi.org/10.1002/jmv.25827
- [27] Institute for Health Metrics and Evaluation. 2021. COVID-19 Projections for the United States. https://covid19. healthdata.org/united-states-of-america.
- [28] Institute for Health Metrics and Evaluation. 2021. Modeling COVID-19 scenarios for the United States. *Nature Medicine* 27, 1 (2021), 94.
- [29] Jayson S. Jia, Xin Lu, Yun Yuan, Ge Xu, Jianmin Jia, and Nicholas A. Christakis. 2020. Population flow drives spatio-temporal distribution of COVID-19 in China. Nature 582, 7812 (April 2020), 389–394. https://doi.org/10.1038/s41586-020-2284-y
- [30] Dayun Kang, Hyunho Choi, Jong-Hun Kim, and Jungsoon Choi. 2020. Spatial epidemic dynamics of the COVID-19 outbreak in China. International Journal of Infectious Diseases 94 (May 2020), 96–102. https://doi.org/10.1016/j.ijid.2020. 03 076
- [31] Amol Kapoor, Xue Ben, Luyang Liu, Bryan Perozzi, Matt Barnes, Martin Blais, and Shawn O'Banion. 2020. Examining Covid-19 forecasting using spatio-temporal graph neural networks. arXiv preprint arXiv:2007.03113 (2020).
- [32] Firdos Khan, Alia Saeed, and Shaukat Ali. 2020. Modelling and forecasting of new cases, deaths and recover cases of COVID-19 by using vector autoregressive model in pakistan. *Chaos, Solitons & Fractals* 140 (2020), 110189.
- [33] Jackson A. Killian, Marie Charpignon, Bryan Wilder, Andrew Perrault, Milind Tambe, and Maimuna S. Majumder. 2020. Evaluating COVID-19 Lockdown and Business-Sector-Specific Reopening Policies for Three US States. https://teamcore.seas.harvard.edu/files/teamcore/files/covid_19_us_states.pdf.

- [34] İsmail Kırbaş, Adnan Sözen, Azim Doğuş Tuncer, and Fikret Şinasi Kazancıoğlu. 2020. Comparative analysis and forecasting of COVID-19 cases in various European countries with ARIMA, NARNN and LSTM approaches. Chaos, Solitons & Fractals 138 (2020), 110015.
- [35] S.C. Kou, Shihao Yang, Chia-Jung Chang, Teck-Hua Ho, and Lisa Graver. 2020. Unmasking the actual COVID-19 case count. Clinical Infectious Diseases 71, 11 (May 2020), 2949–2951. https://doi.org/10.1093/cid/ciaa580
- [36] Shengjie Lai, Nick W. Ruktanonchai, Liangcai Zhou, Olivia Prosper, Wei Luo, Jessica R. Floyd, Amy Wesolowski, Mauricio Santillana, Chi Zhang, Xiangjun Du, et al. 2020. Effect of non-pharmaceutical interventions to contain COVID-19 in China. *Nature* 585, 7825 (May 2020), 410–413. https://doi.org/10.1038/s41586-020-2293-x
- [37] Mi Lim Lee, David Goldsman, Seong-Hee Kim, and Kwok-Leung Tsui. 2014. Spatiotemporal biosurveillance with spatial clusters: Control limit approximation and impact of spatial correlation. IIE Transactions 46, 8 (May 2014), 813–827. https://doi.org/10.1080/0740817X.2013.785296
- [38] Lu Liu. 2020. Emerging study on the transmission of the novel coronavirus (COVID-19) from urban perspective: Evidence from China. Cities 103 (Aug. 2020), 102759. https://doi.org/10.1016/j.cities.2020.102759
- [39] Los Alamos National Laboratory. 2021. LANL COVID-19 Cases and Deaths Forecasts. https://covid-19.bsvgateway. org/.
- [40] Fred S. Lu, Andre T. Nguyen, Nick Link, and Mauricio Santillana. 2020. Estimating the prevalence of COVID-19 in the United States: Three complementary approaches. medRxiv (2020). https://doi.org/10.1101/2020.04.18.20070821
- [41] Mohsen Maleki, Mohammad Reza Mahmoudi, Darren Wraith, and Kim-Hung Pho. 2020. Time series modelling to forecast the confirmed and recovered cases of COVID-19. Travel Medicine and Infectious Disease 37 (2020), 101742.
- [42] Bin Meng, Jinfeng Wang, J. Liu, J. Wu, and E. Zhong. 2005. Understanding the spatial diffusion process of severe acute respiratory syndrome in Beijing. *Public Health* 119, 12 (Dec. 2005), 1080–1087. https://doi.org/10.1016/j.puhe.2005.02. 003
- [43] U.S. News. 2021. COVID-19 Deaths per 100K. https://www.usnews.com/news/best-states/coronavirus-data/covid-death-rate?chart_type=map.
- [44] Northeastern University, Laboratory for the Modeling of Biological and Socio-Technical Systems. 2021. COVID-19 Modeling. https://covid19.gleamproject.org/.
- [45] Graziano Onder, Giovanni Rezza, and Silvio Brusaferro. 2020. Case-fatality rate and characteristics of patients dying in relation to COVID-19 in Italy. JAMA 323, 18 (March 2020), 1775–1776. https://doi.org/10.1001/jama.2020.4683
- [46] Canelle Poirier, Dianbo Liu, Leonardo Clemente, Xiyu Ding, Matteo Chinazzi, Jessica Davis, Alessandro Vespignani, and Mauricio Santillana. 2020. Real-time forecasting of the COVID-19 outbreak in Chinese provinces: Machine learning approach using novel digital data and estimates from mechanistic models. *Journal of Medical Internet Research* 22, 8 (2020), e20285. https://doi.org/10.2196/20285
- [47] Canelle Poirier, Wei Luo, Maimuna S. Majumder, Dianbo Liu, Kenneth Mandl, Todd Mooring, and Mauricio Santillana. 2020. The role of environmental factors on transmission rates of the COVID-19 outbreak: An initial assessment in two spatial scales. Available at SSRN: https://ssrn.com/abstract=3552677. (March 2020).
- [48] The COVID Tracking Project. 2020. About the Project. https://covidtracking.com/about.
- [49] Evan L. Ray, Nutcha Wattanachit, Jarad Niemi, Abdul Hannan Kanji, Katie House, Estee Y. Cramer, Johannes Bracher, Andrew Zheng, Teresa K. Yamana, Xinyue Xiong, et al. 2020. Ensemble forecasts of coronavirus disease 2019 (COVID-19) in the US. MedRXiv (2020).
- [50] Santanu Roy, Gouri Sankar Bhunia, and Pravat Kumar Shit. 2020. Spatial prediction of COVID-19 epidemic using ARIMA techniques in India. Modeling Earth Systems and Environment 7, 2 (2020), 1–7.
- [51] Amal I. Saba and Ammar H. Elsheikh. 2020. Forecasting the prevalence of COVID-19 outbreak in Egypt using nonlinear autoregressive artificial neural networks. *Process Safety and Environmental Protection* 141 (2020), 1–8.
- [52] Mohammad M. Sajadi, Parham Habibzadeh, Augustin Vintzileos, Shervin Shokouhi, Fernando Miralles-Wilhelm, and Anthony Amoroso. 2020. Temperature and latitude analysis to predict potential spread and seasonality for COVID-19. Available at SSRN: https://ssrn.com/abstract=3550308. (March 2020). https://doi.org/10.2139/ssrn.3550308
- [53] Ram Kumar Singh, Meenu Rani, Akshaya Srikanth Bhagavathula, Ranjit Sah, Alfonso J. Rodriguez-Morales, Himang-shu Kalita, Chintan Nanda, Shashi Sharma, Yagya Datt Sharma, Ali A. Rabaan, et al. 2020. Prediction of the COVID-19 pandemic for the top 15 affected countries: Advanced autoregressive integrated moving average (ARIMA) model. JMIR Public Health and Surveillance 6, 2 (2020), e19115.
- [54] Tanu Singhal. 2020. A review of coronavirus disease-2019 (COVID-19). Indian Journal of Pediatrics 87, 4 (March 2020), 281–286. https://doi.org/10.1007/s12098-020-03263-6
- [55] S.K. Tamang, P.D. Singh, and B. Datta. 2020. Forecasting of Covid-19 cases based on prediction using artificial neural network curve fitting technique. *Global Journal of Environmental Science and Management* 6, Special Issue (Covid-19) (2020), 53–64.
- [56] The University of Texas COVID-19 Modeling Consortium. 2021. COVID-19 Mortality Projections for US States. https://covid-19.tacc.utexas.edu/dashboards/us/.

33:20 S. Zhu et al.

[57] The New York Times. 2020. We're Sharing Coronavirus Case Data for Every U.S. County. https://www.nytimes.com/article/coronavirus-county-data-us.html.

- [58] Spencer Woody, Mauricio Garcia Tec, Maytal Dahan, Kelly Gaither, Michael Lachmann, Spencer Fox, Lauren Ancel Meyers, and James G. Scott. 2020. Projections for first-wave COVID-19 deaths across the US using social-distancing measures derived from mobile phones. *medRxiv* (2020).
- [59] Zifeng Yang, Zhiqi Zeng, Ke Wang, Sook-San Wong, Wenhua Liang, Mark Zanin, Peng Liu, Xudong Cao, Zhongqiang Gao, Zhitong Mai, et al. 2020. Modified SEIR and AI prediction of the epidemics trend of COVID-19 in China under public health interventions. *Journal of Thoracic Disease* 12, 3 (March 2020), 165–174. https://doi.org/10.21037/jtd.2020. 02.64
- [60] Zhuowen Zhao, Kieran Nehil-Puleo, and Yangzhi Zhao. 2020. How well can we forecast the COVID-19 pandemic with curve fitting and recurrent neural networks? *medRxiv* (2020).

Received September 2020; revised May 2021; accepted May 2021